Journal of Hazardous Materials 192 (2011) 62–70

Contents lists available at ScienceDirect

Journal of Hazardous Materials

journal homepage: www.elsevier.com/locate/jhazmat

Removal of malachite green by adsorption and precipitation using aminopropyl functionalized magnesium phyllosilicate

Young-Chul Lee [a], Eui Jin Kim [b], Ji-Won Yang [a], Hyun-Jae Shin [b,*]

[a] Department of Chemical and Biomolecular Engineering (BK21 Program), KAIST, 335 Gwahak-ro, Yuseong-gu, Daejeon 305-701, Republic of Korea
[b] Department of Chemical and Biochemical Engineering, Chosun University, Seosuk-dong, Dong-gu, Gwangju 501-759, Republic of Korea

ARTICLE INFO

Article history:
Received 7 February 2011
Received in revised form 11 April 2011
Accepted 25 April 2011
Available online 6 May 2011

Keywords:
Malachite green
Adsorption
Precipitation
Phyllosilicate
Wastewater treatment

ABSTRACT

We report a method for the removal of malachite green (MG) by adsorption and precipitation using nano-sized aminopropyl functionalized magnesium phyllosilicate (AMP) clay. MG, which is used in aquaculture and fisheries, is a carcinogenic and mutagenic compound. In response to these health risks, many efforts have been focused on adsorption of MG onto various adsorbents, which is a versatile and widely used technique for removing MG from water. Herein, we describe the adsorption and precipitation of MG using AMP clay, as well as the alkaline fading phenomenon of MG. In this study, prepared AMP clay and the precipitate product after the reaction of MG–AMP clay mixture were characterized. In addition, adsorption isotherms and kinetics, as well as thermodynamic studies are presented. Based on the results, we suggest a macro- and microscopic removal mechanism for the adsorption and precipitation of MG using AMP clay. An AMP clay dosage of 0.1 mg mL^{-1} exhibited a maximum removal capacity of 334.80 mg g^{-1} and 81.72% MG removal efficiency. With further increases of the AMP clay dosage, removal capacity by AMP clay gradually decreased; at dosage above 0.2 mg mL^{-1} of AMP clay, the removal efficiency reached 100%.

1. Introduction

Malachite green (MG) is a basic dye that has been used for dyeing wool, silk, leather and cotton as well as a fungicide and ectoparasiticide in aquaculture and fisheries it is generating environmental concerns [1]. Not only the colors of the dyes affect the penetration of sunlight into streams, but also the dye is carcinogenic and mutagenic [2,3]. Due to the considerable resistance of MG to biodegradation, physical and chemical processes for MG removal have been widely studied. Characteristics of the removal procedures that have been investigated include removal capacity, treatment cost, and operating conditions, among other factors [4–6]. Chemical treatment technology is costly and involves complex processes that generate toxic by-products [7]. Therefore, alternative physical methods for MG removal have been widely studied. Using low cost adsorbents of silica based materials, such as clay and its derivatives, may be a good approach because of their large surface area and high cationic exchange capacity [8,9]. Other adsorbents, such as ash [10], chitosan [11], cyclodextrin [12], activated carbon [13,14], hen feathers [15], plant leaves [16], chlorella [17], de-oiled soya [18], and algae [19], have been successfully evaluated with regard to their ability for physical removal of MG. However, many of these studies have not considered the alkaline fading phenomenon of MG. Recently, Samiey and Toosi detailed the MG alkaline fading phenomenon [20–22], and specifically reported that cationic chromatic MG was changed into a white precipitate carbinol base at an alkaline pH. As shown in Fig. 1, three forms of MG can exist; leuco MG is formed when MG penetrates into the human body. However, we will consider only chromatic MG and MG carbinol base, which is MG form in alkaline pH condition in aqueous systems. When MG is removed by adsorbents under an alkaline solution, the MG carbinol base in precipitate form should be considered [22]. More recently, clay minerals of layered organo-inorganic hybrid materials, resembling the talc parent structure $Si_8Mg_6O_{20}(OH)_4$, have been synthesized by a sol–gel reaction at ambient conditions with various combinations of metal ions, such as magnesium [23,24], nickel [25], and zinc [26]. Organo-functionalities of above clays have been extensively investigated from an academic as well as an applied perspective. Mann and colleagues further synthesized organoclay (AMP clay) as 2:1 trioctahedral typed aminopropyl magnesium (organo)phyllosilicate. AMP clay can be synthesized by a one-pot sol–gel reaction in ambient conditions by controlling centered metal ions and sandwiched organo-functionalities [27,28]. This process results in organo-building blocks that are optically transparent due to the repulsion of protonated amine groups in aqueous media. The cationic and water-solubilized properties of AMP clay in aqueous solutions have been utilized to construct hybrid

* Corresponding author. Tel.: +82 62 230 7518; fax: +82 62 230 7226.
E-mail address: shinhj@chosun.ac.kr (H.-J. Shin).

0304-3894/$ – see front matter © 2011 Elsevier B.V. All rights reserved.
doi:10.1016/j.jhazmat.2011.04.094

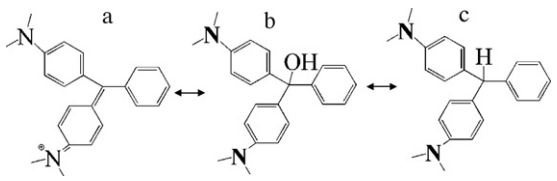

Fig. 1. Three forms of malachite green (MG): chromatic malachite green (a), carbinol base (b), and leuco malachite green (c).

materials with biomolecules [29–32] and Schiff bases [33], dye labeling for cellular uptake [34], and drug delivery systems [35].

Unfortunately, artificial AMP clays have not been applied toward pollutant clean-up, even though their cationic and ammonium properties in aqueous solutions merit the feasibility of such an approach. Herein, we report, for the first time, the adsorption and precipitation of MG using the positively charged organo-building blocks of nano-sized AMP clay sheets. The specific goals of this study were (1) to prepare and characterize AMP clay and the MG–AMP clay mixture, (2) to suggest a removal mechanism that includes adsorption, precipitation, MG fading, and collapsing of the AMP clay structure, and (3) to present the adsorption kinetics and a thermodynamic study of the MG–AMP clay mixture.

2. Experimental

2.1. Materials

The cationic dye, MG oxalate (C.I. Basic Green 4, C.I. Classification Number 42,000, $C_{52}H_{54}N_4O_{12}$, M.W. = 927.00, λ_{max} = 617 nm) and 3-aminopropyltriethoxysilane (APTES, 99%) were supplied by Sigma–Aldrich (St. Louis, MO, USA) and used without further purification, unless otherwise specified. Ethanol (>99.9%) was purchased from Merck KGaA (Darmstadt, Germany). Magnesium chloride hexahydrate (98.0%) was obtained from Junsei Chemical Co. Ltd. (Tokyo, Japan). HCl or NaOH (1.00 M or 0.10 M) standard solutions were purchased from Dae Jung Chemicals (Shiheung, Korea) to adjust the final pH of samples.

2.2. Preparation of AMP clay

For AMP clay preparation, we followed methods that have been previously reported in the literature [30,31,34,35]. Specifically, magnesium chloride hexahydrate (0.84 g) was dissolved in 20 g of ethanol and 1.3 mL of APTES added to this solution, where the intended molar ratio of Mg to Si is 0.75, with continuous stirring. A white colored precipitate gradually formed within 10 min and was stirred overnight for the reaction to reach completion. The

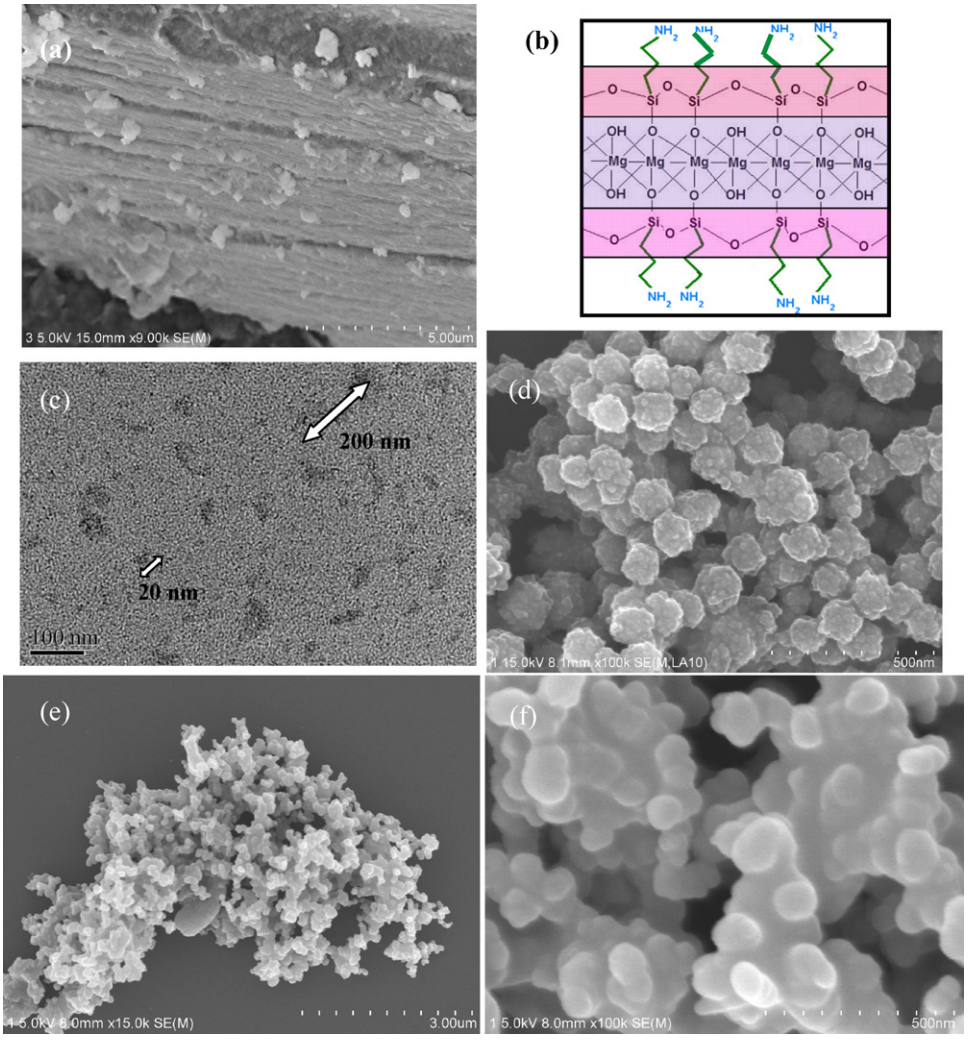

Fig. 2. SEM/TEM images of AMP clay and precipitate of MG–AMP clay mixture. (a) SEM image of powder AMP clay, (b) a schematic unit structure of AMP clay, (c) TEM image of diluted AMP clay sheets in aqueous solution on carbon-coated copper grid, (d) SEM image of the precipitated carbinol base, and (e) SEM images of low magnification and (f) high magnification of MG–AMP clay mixture.

Table 1
Results of ICP-AES measurement of AMP clay and MG in aqueous solution.

Name	Weight (mg mL^{-1})	Mg (mg L^{-1})	Si (mg L^{-1})
AMP	1	2.712	5.953
MG with AMP	1	0.009	0.233
DI water	–	0.009	0.008

precipitate was collected by centrifugation, washed three times with ethanol (50 mL) to remove excess magnesium chloride, and dried overnight at 313 K.

2.3. Preparation of MG stock solution

The stock solution (3×10^{-1} mM of MG) was prepared by dissolving an accurately weighed 278.1 mg of dye in de-ionized distilled water (DI water). MG standard solutions were diluted to each desired concentration using DI water.

2.4. MG removal

To study the pH effect on MG removal, 1.0 mg of AMP clay was agitated with 10 mL of dye solution (3×10^{-3} mM) at room temperature. The experiments were conducted at different pH levels, from 3 to 10. Agitation was carried out at a constant agitation speed of 130 rpm for 120 min (see supporting information, Fig. S1), which was sufficient to reach equilibrium. As the pH increased, the peak of chromatic MG at 617 nm decreased while the peak at 255 nm of carbinol base increased. After 120 min, the samples

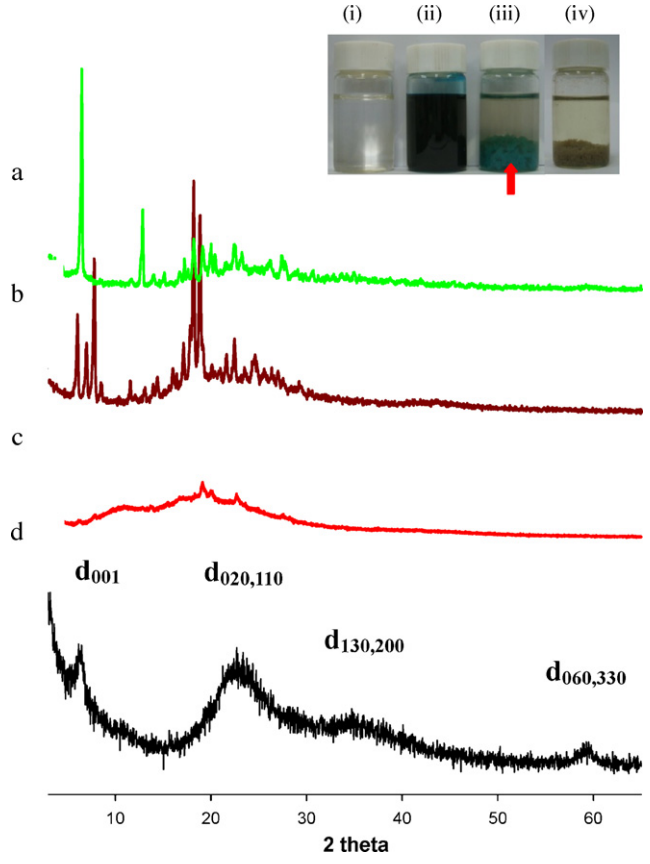

Fig. 3. PXRD patterns of (a) mechanical mixing of AMP clay powder and MG powder, (b) MG powder, (c) MG–AMP clay mixture, and (d) AMP clay. Inset shows (i) photographs of exfoliated AMP clay in aqueous solution, (ii) MG in aqueous solution, (iii) AMP clay–MG mixture after 10 min, and (iv) MG–AMP clay mixture after 1 week. *Note*: (c) was PXRD of inset (iii). *y*-Axis indicates counts/s.

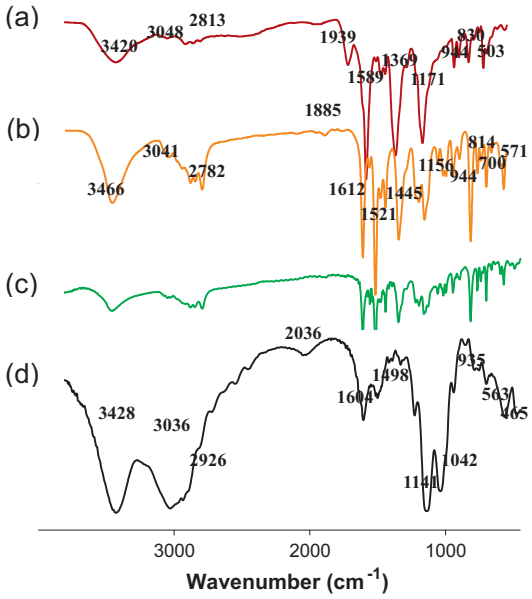

Fig. 4. FTIR spectra of (a) MG powder, (b) carbinol base powder, (c) precipitate product of MG–AMP clay mixture, and (d) AMP clay powder. *y*-Axis indicates transmittance (%).

were centrifuged at 6000 × *g* for 20 min and then directly measured using a UV–Vis spectrophotometer. In order to confirm equilibrium condition, we measured the UV–Vis spectra at 120 min and 240 min, indicating the peaks are almost constant (see supporting information, Fig. S2). The pH of the solution was adjusted by dropwise addition of HCl or NaOH (0.10 M) standard solutions and measured using a pH meter (Thermo Orion, Model 710, USA).

To examine the effect of AMP clay for MG removal, 1.0–14.0 mg of AMP clay was added to 10 mL dye solution (3×10^{-3} mM concentration) while stirring (250 rpm) at room temperature overnight. The removal capacity (q_e, mg g^{-1}) was defined as the amount of MG molecules adsorbed divided by the AMP clay loading at equilibrium:

$$q_e = \frac{V(C_0 - C_e)}{W}$$

where V (L) is the volume of the sample treated, C_0 (mg L^{-1}) and C_e (mg L^{-1}) are the initial concentration and equilibrium MG concentration, respectively in the liquid phase, and W (g) is the amount of AMP clay. The removal efficiency (%) was calculated as follows:

$$\frac{C_0 - C_{su}}{C_0} \times 100$$

where C_0 (mg L^{-1}) is the initial dye concentration and C_{su} (mg L^{-1}) is the supernatant MG concentration after centrifugation (6000 × *g* for 20 min). The control experiments (with and without MG) were performed under the same conditions.

2.5. Adsorption isotherms

Adsorption isotherms were determined using the batch equilibrium method. For batch adsorption experiments, 0.1 mg mL^{-1} of AMP clay was applied when evaluating the maximum removal capacity (q_e), where the MG concentration in aqueous solution was 3×10^{-3} mM. The solutions were shaken for 120 min at room temperature; at that time final pH was approximately 9.8. Then the aliquots were collected after centrifugation from the samples at 6000 × *g* for 20 min. And then supernatants were recorded using a UV–Vis spectrophotometer at 617 nm (λ_{max}) to calculate dye

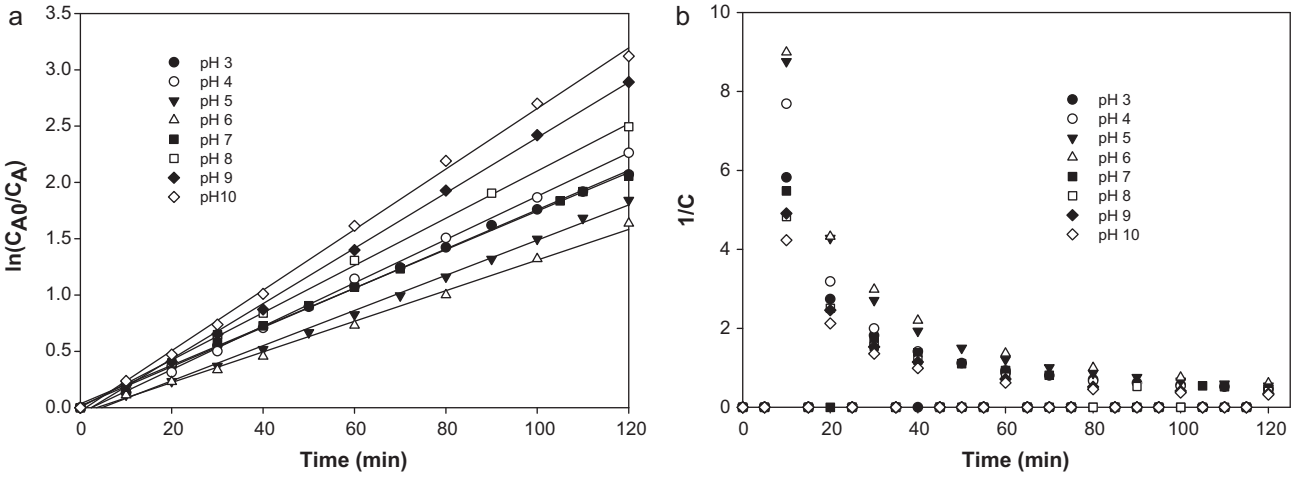

Fig. 5. Pseudo-first-order (a) and pseudo-second-order kinetic plots of MG removal with AMP clay as a function of initial pH; initial MG concentration: 3×10^{-3} mM, AMP clay concentration: 0.1 mg mL^{-1}.

concentration. The precipitate amount of MG–AMP clay mixture was calculated based on the intensity difference between the initial and equilibrium concentrations of MG.

2.6. Removal kinetics and thermodynamics

The kinetics of MG removal using AMP clay was also investigated using the batch processing mode. 10 mL of MG solution and 1 mg of AMP clay were mixed in airtight 15 mL conical tubes. To retain the reaction temperature, the conical tubes were kept in a water bath with constant agitation (293.15, 313.15, and 333.15 K). At proper time intervals, samples were collected from the supernatants after centrifugation and were directly recorded using a UV–Vis spectrophotometer. All the experiments were conducted in duplicate; the data presented therefore reflect the mean of duplicate analyses.

2.7. Characterizations of AMP clay and its mixture

The surface morphologies of the samples were observed using a field emission scanning electron microscope (FE-SEM, Sirion Instrument, FEI Com/Noran, Netherlands) with attached energy dispersive X-ray (EDX) analysis and transmission electron microscopy (TEM, JEM-2100F HR, 200 kV). Powder X-ray diffraction (PXRD) data were obtained on a Rigaku D/max lllC (3 kW) with a θ/θ goniometer equipped with a CuKα radiation generator at 40 kV and 45 mA. The scan range was from 3° to 65° at a rate of 1.2° 2θ min^{-1}. A small-angle X-ray diffractometer (SAXS) measures were obtained using a D/MAX-2500 (Rigaku, $2\theta = 0.25$–6). UV–Vis spectra (200–750 nm) were recorded in survey scan mode with 2 nm of interval wavelength (Optizen 3220UV, Mecasys, Korea). The particle size distribution of the exfoliated dispersion of AMP clay sheets in aqueous solution was examined by a laser scattering particle size analyzer (HELOS/RODOS & SUCELL, Germany). AMP clay in aqueous solution was sonicated for 5 min, becoming optically transparent (water-soluble), and then measurement of Mg and Si concentrations was performed using an ICP-AES (JY70PLUS, Jovin-Yvon, France). Fourier transform infrared (FT-IR) spectrometry of KBr pellets (FT-IR 4100, Jasco, Japan) was collected from 4000 cm^{-1} to 450 cm^{-1}.

3. Results and discussion

3.1. Electron microscopy observations and composition analysis

The powder morphology of AMP clay is shown in Fig. 2a; the clay had a layered structure with approximately 1.8 nm of regular layer distance, which was roughly estimated based on scale

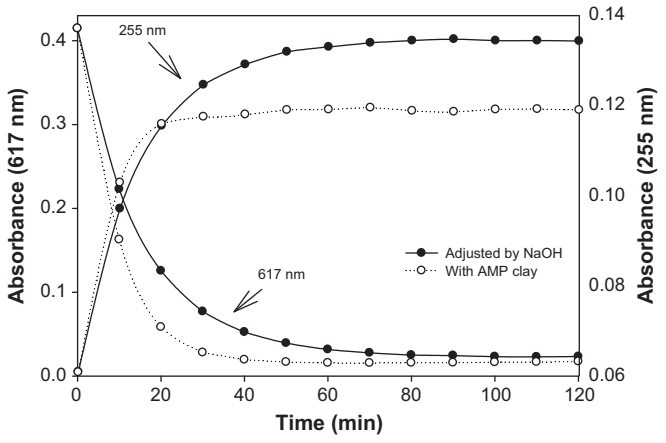

Fig. 6. UV–Vis absorption spectra of MG with NaOH or with AMP clay at pH 9.8 as a function of time; initial MG concentration: 3×10^{-3} mM, AMP clay concentration: 0.1 mg mL^{-1}.

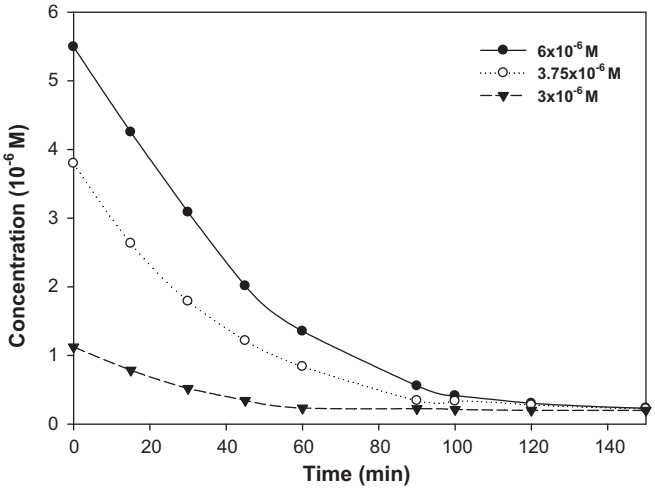

Fig. 7. Removal kinetics of different initial concentrations of MG at temperature 293.15 K.

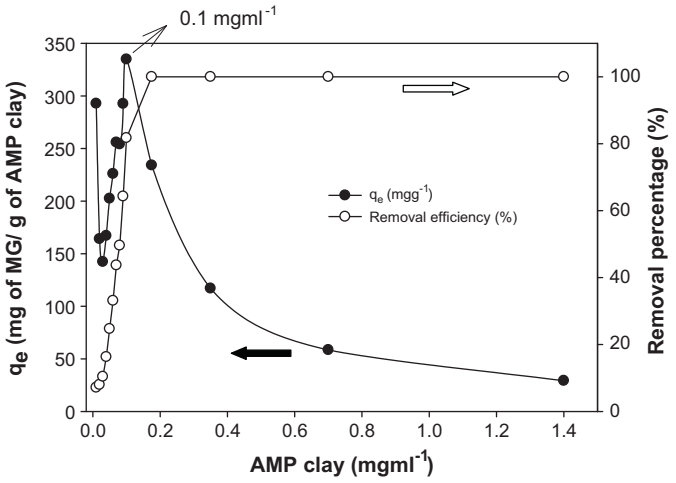

Fig. 8. Removal capacity (q_e, mg g^{-1}) and removal efficiency (%) of MG with AMP clay loading at pH 9.8.

bar. The approximate unit cell structure of AMP clay is depicted in Fig. 2b. A TEM image of the organo-building blocks of exfoliated dispersion of AMP clay sheets in aqueous solution is shown in Fig. 2c; the diameters of the AMP clay sheets ranged from 20 nm to 200 nm, which is in the range previously reported in the literature [30,31,34]. From the TEM images, observed under dry conditions, we observed a larger sample size than that in aqueous solution. To further investigate the size of organo-building blocks of AMP clay sheets in aqueous solution we measured that by the dynamic light scattering (DLS). The resulting cumulative probability size at 99% (X_{99}) of organo-building blocks of AMP clay sheets showed in aqueous solution an average diameter of 64.60 nm with surface and volume average diameters of 43.74 nm and 44.93 nm, respectively (see supporting information, Fig. S3) where two mean diameters were obtained based on specific surface area ($m^2\ g^{-1}$) and specific volume ($m^3\ g^{-1}$), which can be interpreted that the larger ratio of surface to volume diameter, the more spherical particle of dispersed AMP clay sheets. AMP clay sheets in the aqueous solution exhibited a nano-sized distribution in the range of visible light. As a reference, the morphology of the precipitated carbinol base of MG exhibited uniform spherical structures, as shown in Fig. 2d. Fig. 2e and f shows SEM images of the precipitated carbinol base on the AMP clay plates in low and high magnifications, respectively. AMP clay exhibited good transparency in a wide pH range. However, the induction of the carbinol base of MG caused the precipitation of

Table 2
Langmuir and Freundlich adsorption isotherm parameters of MG on AMP clay sheets at 293.15 K temperature.

Langmuir isotherm			Freundlich isotherm		
Q_{max}	K_L	R^2	K_f	n	R^2
130.64	-1.12×10^3	0.92	1137.97	−2.51	0.52

macro-sized plates of AMP clay with a decorated or partially buried carbinol base of MG (Fig. 2e and f). In addition to the observation of the micrographs, we confirmed the compositions of AMP clay and MG–AMP clay mixture. The AMP clay was 18.3% C, 5.6% H, 6.7% N, and 9.4% O. In contrast, MG–AMP clay mixture exhibited a 78.1% increase of C and an 8.0% increase of N, due to the MG molecular structure (see supporting information, Table S1). Based on the EDX analysis of AMP clay, the ratio of Mg to Si showed *ca.* 0.53 (see supporting information, Table S2). We further confirmed the concentration of magnesium and silica in the AMP clay using ICP-AES equipment, resulting in *ca.* 0.46 of the ratio of Mg to Si (Table 1). However, in the case of MG–AMP clay mixture, the concentration of magnesium, which is the centered cationic ion of AMP clay, significantly decreased. This indicates that the AMP clay structure was collapsed and dissociated by the microenvironment around the MG. In the presence of MG molecules, 0.1 mg mL^{-1} of AMP clay was precipitated in 10 min of reaction time. The silicon concentration in the sediment of the sample increased while the magnesium concentration slightly decreased (see supporting information, Fig. S4).

3.2. PXRD pattern

As displayed in Fig. 3d, the AMP had a layered structure with a 1.4 nm base spacing of d_{001} with broad peaks over higher angles. Basal spacing is smaller than that of SEM image, but this value is accurate. Moreover the $d_{060,330}$ peak indicated 2:1 trioctahedral phyllosilicate at $2\theta = 59^\circ$, corresponding to previously reported results [28,31,32,34,35]. However, MG–AMP clay mixture after precipitation showed irregular and amorphous silica structures. The sharp peaks of cabinol base were significantly reduced by silica materials. In addition, the peak of the 2:1 trioctahedral unit structure disappeared; indicating that the basic unit of structure had collapsed. While sharp peaks of crystalline MG were initially observed (Fig. 3b), the intense sharp peaks of MG disappeared after the reaction (Fig. 3c), indicating that MG was significantly removed by the AMP clay. For control experiment, according to Fig. 3a the physical mixing of MG and AMP clay powders showed sharp and

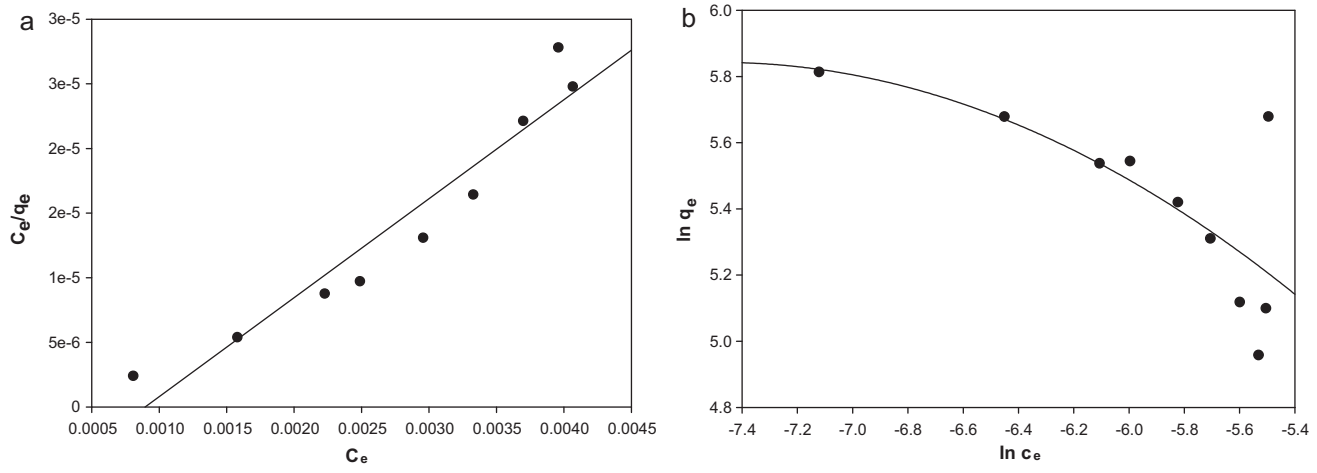

Fig. 9. Langmuir (a) and Freundlich (b) adsorption isotherms of MG with AMP clay.

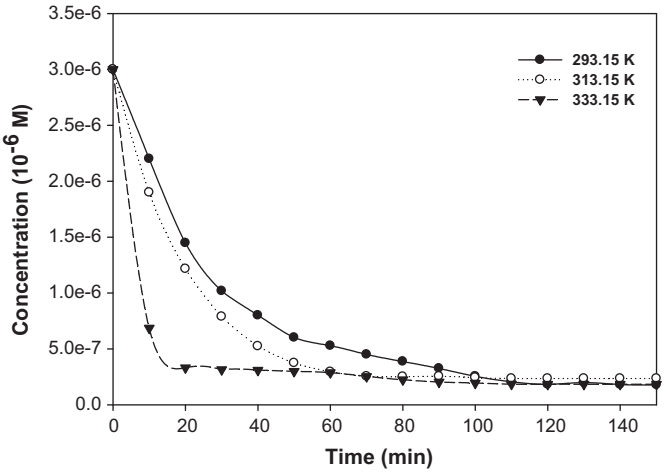

Fig. 10. Kinetics of MG with AMP clay according to temperature; initial MG concentration: 3×10^{-3} mM, AMP clay concentration: 0.1 mg mL^{-1}.

new peaks at 6.44, 12.80 of 2θ, while MG showed 5.99, 6.95, 7.76, 18.14, and 18.83 of 2θ. These findings also support the collapse of the AMP clay unit structure by MG, as observed from the micrographs of AMP clay with MG (Fig. 2e and f). Fig. 3 and the inset data indicate that MG was precipitated by AMP clay and changed the white color of the carbinol base after 1 day, ultimately resulting in a gray precipitated MG with silica materials from the AMP clay.

3.3. FTIR spectra

The FTIR spectra of MG, carbinol base, precipitate of MG–AMP clay mixture, and AMP clay are shown in Fig. 4. The broad band at 3428 cm^{-1} of –OH stretching vibration spectrum of AMP clay (Fig. 4d) was shifted to 3466 cm^{-1} in MG–AMP clay mixture by interaction with carbinol base (Fig. 4c). Characteristic bands of AMP clay were –CH_2– (3036 cm^{-1}), –NH_3^+ (2036 cm^{-1}), –NH_2 (1604 cm^{-1}), –CH_2 (1498 cm^{-1}), Si–C (1141 cm^{-1}), Si–O–Si (1042 cm^{-1}), and Mg–O (465 cm^{-1}) (Fig. 4d). These peaks are in good agreement with previous reports [30,31,34]. The assigned –CH– stretching vibration of AMP clay was also shifted from 3036/2926 cm^{-1} to 3041/2782 cm^{-1} by the effect on carbinol base. Interestingly, the peaks of carbinol base (Fig. 4b) and MG–AMP clay mixture (Fig. 4c) were almost similar, meaning that MG existed as carbinol base in MG–AMP clay mixture [36]. The –NH_3^+ peak of AMP clay disappeared after the reaction with MG, indicating that amine groups of AMP clay were involved in the reaction with carbinol base through hydrogen bonding. The N–H bending vibrations at 1604/1498 cm^{-1} of AMP clay were shifted to 1612/1521 cm^{-1}. Conclusively, carbinol base (not MG form) and AMP clay were significantly interacted with each other in the microenvironment because AMP clay made the aqueous solution alkaline.

3.4. Effect of pH on MG removal

pH is a significant parameter for the removal of MG by AMP clay because protons enhance the degree of protonated dispersion of AMP clay sheets and the alkaline fading of MG in an aqueous solution. The effect of different initial pH values on the removal of MG by AMP clay was investigated at AMP clay loading of 0.1 mg mL^{-1}. The removal capacity (334.80 mg g^{-1}) and the adsorption equilibrium time (120 min) were not changed where MG removal included the precipitation at alkaline condition; however, the removal rate decreased when the initial pH of the MG was acidic (data not shown). We observed that the rate of MG removal by AMP clay decreased in the following order: pH 10 > pH 9 > pH 8 > pH 4 > ≈pH 7 > pH 5 ≈ pH 6 (Fig. 5). This can be explained by that the absorbance intensity (617 nm) of MG in aqueous solution was changed by pH shift (see supporting information, Fig. S5). Therefore, under alkaline pH, removal rate was fast, and then pH 4 and pH 7 would be followed. The pH 5–6 is the pH of MG without pH adjustment.

This can be explained that AMP clay in aqueous solution showed a positively charged surface potential under a wide pH range [30,31,34]. The MG showed cationic properties below weak acid, and a neutral carbinol base predominantly existed above neutral pH [17]. For MG behavior in the presence of AMP clay, as shown in Fig. 6, the peak at 617 nm of MG disappeared faster in the presence of AMP clay than under the NaOH adjustment at the same pH (9.8). The solution pH was spontaneously changed into 9.8 after the addition of AMP clay. Simultaneously, the peak at 255 nm of the carbinol base with AMP clay increased faster than that for the NaOH adjustment. Comparing with and without AMP clay at the same pH condition, AMP clay accelerated the precipitation of MG as a carbinol base type.

3.5. Effect of initial MG concentration and AMP clay loading

As shown in Fig. 7, the effect of the initial concentrations of MG (6, 3.75, 3, and 1.2×10^{-6} M) on MG removal was examined with 0.1 mg mL^{-1} of AMP clay for 180 min. The removal pattern of MG

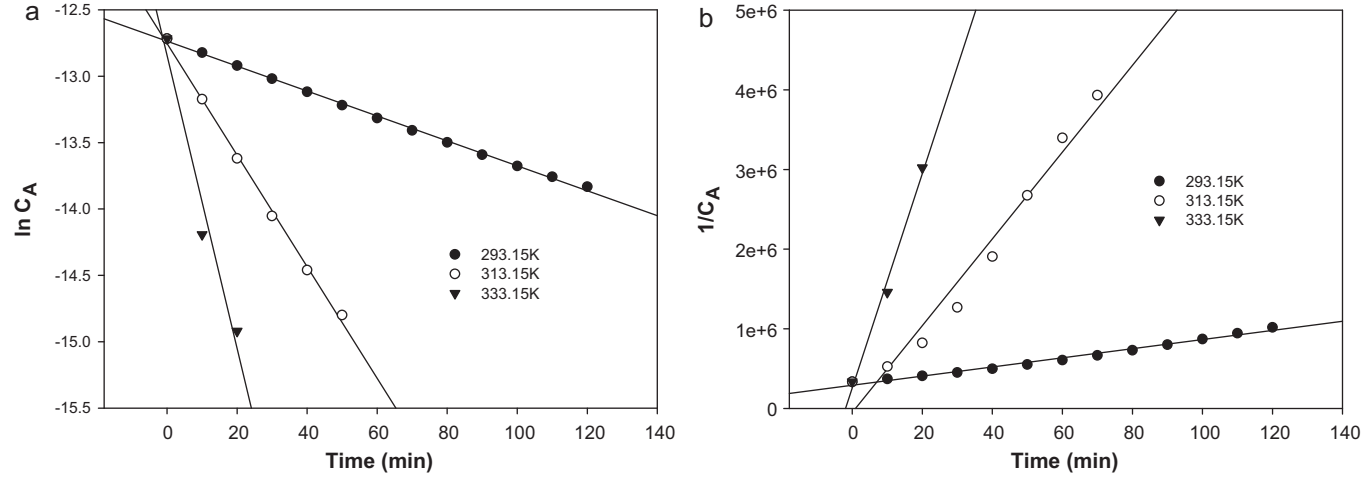

Fig. 11. Thermodynamic study of MG with AMP clay, pseudo-first-order reaction (a) and pseudo-second-order reaction (b), initial MG concentration: 3×10^{-3} mM, AMP clay concentration: 0.1 mg mL^{-1}.

Table 3
Adsorption kinetic parameters of MG with AMP clay at 293.15 K temperature.

T (K)	Pseudo-first-order		Pseudo-second-order	
	k_1 (min^{-1})	R_1^2	k_2 (g mg^{-1} min^{-1})	R_2^2
293.15	9.38×10^{-3}	0.99	5735.08	0.98

Table 4
Thermodynamic parameters for MG with AMP clay.

T (K)	E_a (kJ mol^{-1})	ΔH° (kJ mol^{-1})	ΔS° (kJ mol^{-1})	ΔG° (kJ mol^{-1})
293.15	50.19	47.74	-97.69×10^{-2}	334.14
313.15		47.58	-97.72×10^{-2}	353.28
333.15		47.41	-97.84×10^{-2}	373.40

gradually decreased in all cases. We selected the initial MG concentration of 3×10^{-3} mM for the entire experiment at 0.1 mg mL^{-1} of AMP clay loading because equilibrium was achieved in this condition within 120 min.

The effect of AMP clay loads ranging from 1 to 14 mg on the removal of MG was also studied (Fig. 8). As AMP clay loading increased, the increasing surface area and active sites of AMP clay led to an increase in MG removal efficiency. 0.1 mg mL^{-1} of AMP clay loading exhibited a maximum removal capacity (q_e) of 334.80 mg g^{-1} with 81.72% MG removal efficiency. As we further increased AMP clay loading, the removal capacity of AMP clay gradually decreased, yet above 0.2 mg mL^{-1} of AMP clay the removal efficiency reached nearly 100%. The gradual reduction of removal capacity can be explained by the fact that the amount of MG (per unit weight of AMP clay) was split with the increase in AMP clay, resulting in an exponentially decreasing curve [5]. Therefore, the optimum dosage of AMP clay was 0.1 mg mL^{-1} at of 3×10^{-3} mM concentration of 10 mL MG solution.

3.6. Adsorption isotherms

MG removal by AMP clay included adsorption and precipitation of MG–AMP clay mixture, as well as MG alkaline fading. The whole process can be considered a pseudo-adsorption process. Therefore, a fundamental equilibrium isotherm study is important when considering MG removal by AMP clay. As shown in Fig. 9, based on Langmuir theory, the linear equation for this process is the following:

$$\frac{C_e}{q_e} = \frac{1}{bq_m} + \frac{C_e}{q_m}$$

where q_m (mg g^{-1}) is the monolayer adsorption capacity and b (L mg^{-1}) represents the Langmuir isotherm coefficient. The Freundlich model is distinguished as multilayer adsorption process. The equation for this process is the following:

$$q_e = K_f C_e^{1/n}$$

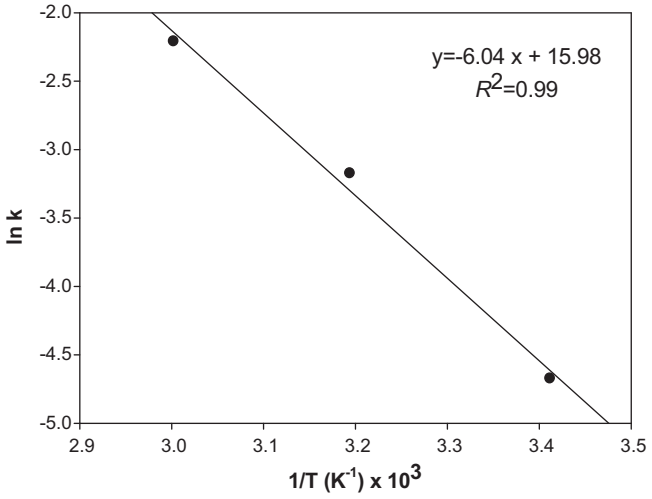

Fig. 12. Arrhenius plot of MG with AMP clay, initial MG concentration: 3×10^{-3} mM, AMP clay concentration: 0.1 mg mL^{-1}.

where K_f (mg g^{-1}) and n are Freundlich constants. Adsorption parameters in this system are summarized in Table 2, using the equilibrium adsorption study with Langmuir and Freundlich models. The linearization of the Langmuir equation was plotted as $y = 7.65 \times 10^{-3}x - 6.85 \times 10^{-6}$ ($R^2 = 0.92$). The q_m value of MG–AMP clay mixture was 130.64 mg g^{-1}. The smaller correlation value may be due to the removal of MG by alkaline fading. However, the correlation coefficient (R^2) of the Freundlich model was much lower than that of the Langmuir model, indicating that the removal process was better modeled by monolayer adsorption (Langmuir) than by multilayer adsorption (Freundlich). Therefore, based on a Langmuir type model, the favorable or unfavorable reactions can be classified by the separation factor, R_L, which is an evaluation parameter of the adsorption capacity [13].

$$R_L = \frac{1}{1 + bC_0}$$

where b (L mg^{-1}) is the Langmuir constant and C_0 (mg L^{-1}) is the initial concentration. The adsorption process can be determined as favorable when the R_L value lies between 0 and 1.

3.7. Effect of temperature

The effect of temperature on MG removal by AMP clay was investigated (Fig. 10). As temperature increased, the time to reach equilibrium was reduced. Specifically, at 293.15, 313.15, and 333.15 K equilibrium conditions were reached in 120, 60, and 20 min, respectively. These may be due to the mass transfer with MG molecules and AMP clay sheets, resulting in fast formation of the carbinol base from chromatic MG. This implies an increased surface activity and kinetic energy of the solute molecules [17]. To examine the adsorption (removal) mechanism of MG–AMP clay mixture, we evaluated pseudo-first-order and a pseudo-secondary-order kinetic model to determine which model was best fit by the experimental data.

The sorption data by Lagergren pseudo-first-order kinetics is based on the followed equation [37]:

$$\frac{d_q}{d_t} = K_1(q_e - q)$$

Integration of the above equation with conditions (q values) at $t = 0$ to $t = t$, results in the following kinetic rate expression:

$$\log(q_e - q_t) = \log_{q_e} - \frac{K_1}{2.303} \times t$$

where K_1 is the pseudo-first-order rate constant (min^{-1}); q_e and q_t are the amounts of MG adsorbed (mg g^{-1}) at equilibrium and at time t (min), respectively.

The pseudo-second-order model can be expressed as [38]:

$$\frac{t}{q_t} = \frac{1}{K_2 q_e^2} + \frac{t}{q_e}$$

where K_2 (g mg^{-1} min^{-1}) is the rate constant of the pseudo-second-order kinetic plot.

Fig. 11 shows the pseudo-first-order and pseudo-second-order kinetic plots as functions of temperature (293.15, 313.15 and 333.15 K). The kinetic constants obtained by linear regression from the two kinetic equations are summarized in Table 3. The

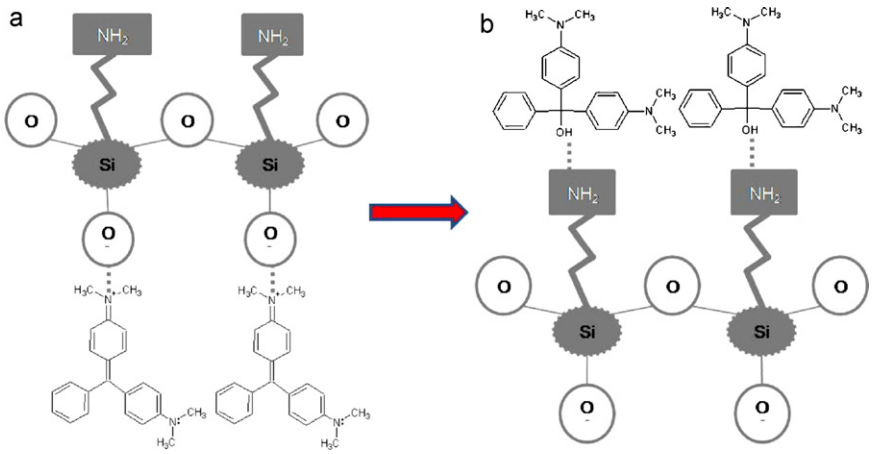

Fig. 13. The proposed MG removal mechanism by AMP clay. Initially (a) positive MG molecules interacted with negatively charged O^- of AMP clay sheets and then (b) OH side of carbinol base interacted at neutral amine group of AMP clay sheets.

correlation coefficient for the pseudo-first-order model is higher ($R^2 = 0.99$) than that for the pseudo-second-order model ($R^2 = 0.98$) at 293.15 K. Thus, the adsorption process followed the pseudo-first-order kinetic model, indicating that the interaction between MG molecules and AMP clays sheets is stronger than that between MG molecules and AMP clay sheets. This result is contrary to results following a pseudo-second-order kinetic model [8,38]. Our finding suggests that AMP clay behaves differently as an adsorbent, showing unique collapsed and precipitated morphology after the precipitation.

3.8. Thermodynamic parameters

In order to determine whether the reactions will proceed spontaneously or not, Gibb's energy and entropy factors have to be considered. If Gibb's energy change (ΔG°) is negative, the reaction process will occur spontaneously. The thermodynamic parameters of the adsorption system are ΔG°, enthalpy change (ΔH°), entropy change (ΔS°), and the equilibrium constant (K). The relationship among these parameters is described by the following equations:

$$\Delta G^\circ = \Delta H^\circ - T\Delta S^\circ$$
$$\Delta G^\circ = -RT \ln K$$

where K (L mol^{-1}) is the equilibrium constant of adsorption, R is the gas constant (8.314 J mol^{-1} K^{-1}), and T is the solution temperature in Kelvin (K). The enthalpy (ΔH°) of MG adsorption by AMP clay was determined by the following equation [5]:

$$\Delta H^\circ = E_a - RT$$

The activation energy (E_a) for MG adsorption by AMP clay was calculated from the Arrhenius equation.

$$\ln k = \ln A - \frac{E_a}{RT}$$

where A is the Arrhenius frequency factor, and k is the rate constant. Fig. 12 is based on the Arrhenius equation. As shown in Table 4, ΔH° is a useful parameter whenever a differential energy change occurs in a system. A positive value greater than 40 kJ mol^{-1} of ΔH° means that the interaction of MG is endothermic in nature and chemisorptions will occur and a negative value of ΔS° shows a decrease in the degrees of freedom, *i.e.*, MG molecules were orderly adsorbed onto AMP clay surfaces. Conclusively, the positive ΔG° indicated that the reaction with MG and AMP clay is not spontaneous. Furthermore, increasing the reaction temperature decreased ΔS°; this indicates that a higher temperature is not energetically favorable and corresponds to an increase of ΔG°. The activation energy, E_a, was obtained from the linear Arrhenius equation, $y = -6.04x + 15.98$ ($R^2 = 0.99$) (Fig. 12). Based on the slope of the graph, E_a was determined to be 50.19 kJ mol^{-1}. The E_a for the interaction of MG–AMP clay mixture was above 40 kJ mol^{-1}; therefore, a chemical adsorption mechanism occurred. This chemical reaction has an energy barrier [11].

3.9. Suggested removal mechanism

Microscopically, a white powder of layered AMP clay, composed of organo-building blocks with at least an average size of 50 nm, was exfoliated in aqueous solution, which increased the pH to 9.8 due to the protonated cationic AMP clay sheets. At acidic pH, chromatic MG showed good dispersion stability, because of electrostatic repulsion, and formed an amorphous structure, not a precipitated one (see supporting information, Fig. S6). However, under alkaline pH, chromatic MG without AMP clay became a carbinol base, which is white in color and of a precipitated form with a spherical morphology. In the MG–AMP clay mixture in aqueous solution, MG was precipitated as a carbinol base of spherical type onto a macro-sized plate-like AMP clay structure (Fig. 2e and f). We presume that the neutrally charged carbinol base induced interactions (adsorption and precipitation) with AMP clay and accelerated precipitation of organo-building blocks of AMP clay sheets in the aqueous solution. AMP clay also helped to change the carbinol base form from MG (Fig. 5). In previous reports using bentonite [8,39] for MG removal process, and anionic dye precipitation by Ca^{2+} and Mg^{2+} ions of alkaline white mud [40], dye removal efficiency increased due to MG alkaline fading, which are different precipitation phenomena comparing with our result. To investigate the interaction of MG molecules and collapsed AMP clay structure, we suggest a possible removal model consisting of electrostatic attraction of positively charged $^+N–(CH_3)_2–$ of MG and negatively charged O^- of silica (Fig. 13a) [5]. And then carbinol base interacted predominantly with amine groups of AMP clay *via* hydrogen bond at alkaline pH (Fig. 13b), which was confirmed by FTIR spectra. The dissociated AMP clay structure was confirmed by measuring Mg and Si concentrations (mg L^{-1}) in the presence of MG as described above. During adsorption and precipitation, both Si and Mg concentrations in the precipitate increased. This means that simultaneous precipitation of MG and structural collapse of AMP clay occurred.

4. Conclusion

In summary, the removal of MG–AMP clay mixture included adsorption of MG onto AMP clay, alkaline fading of MG by AMP

clay, and induced precipitation of MG and AMP clay sheets under basic conditions (pH 9.8). Due to alkaline fading and adsorption of MG, the Langmuir equation led to the predicted adsorption capacity (130.64 mg g^{-1}) but had a correlation (R^2 = 0.92). Adsorption kinetics for MG onto AMP clay was of a pseudo-first-order nature. This indicates that the interaction of MG molecules with AMP clay sheets was stronger than the interaction with each solute. Thermodynamically, MG molecules were orderly arranged onto AMP clay plates and were endothermic in nature. From the above findings, we suggest a removal mechanism model that explains MG removal with AMP clay sheets in aqueous solution. Under pH 9.8, MG becomes a carbinol base and this carbinol base induces synergistic precipitation of exfoliated dispersions of AMP clay sheets. At first, negatively charged O^- of silica interacted positively charged $^+N–(CH_3)_2–$ of MG by electrostatic attraction. And subsequently carbinol base interacted predominantly amine groups of AMP clay *via* hydrogen bond at alkaline pH. We are currently examining desorption (recovery) of MG from the precipitation product by flushing using organic solvents.

Acknowledgement

This work was supported by the research fund from the Chosun University, 2009.

Appendix A. Supplementary data

Supplementary data associated with this article can be found, in the online version, at doi:10.1016/j.jhazmat.2011.04.094.

References

[1] S. Srivastava, R. Sinha, D. Roy, Toxicological effects of malachite green, Aquat. Toxicol. 66 (2004) 319–329.
[2] O. Hernandez-Ramirez, S.M. Holmes, Novel and modified materials for wastewater treatment applications, J. Mater. Chem. 18 (2008) 2751–2761.
[3] G. Crini, Non-conventional low-cost adsorbents for dye removal: a review, Bioresour. Technol. 97 (2006) 1061–1085.
[4] V. Bekiari, P. Lianos, Ureasil gels as a highly efficient adsorbent for water purification, Chem. Mater. 18 (2006) 4142–4146.
[5] C. Kannan, T. Sundaram, T. Palvannan, Environmentally stable adsorbent of tetrahedral silica and non-tetrahedral alumina for removal and recovery of malachite green dye from aqueous solution, J. Hazard. Mater. 157 (2008) 137–145.
[6] O. Martínez-Zapata, J. Méndez-Vivar, P. Bosch, V.H. Lara, Tapping organic molecules in sol–gel aluminosilicate matrices, J. Non-Cryst. Solids 355 (2009) 2496–2502.
[7] Y. Ju, S. Yang, Y. Ding, C. Sun, A. Zhang, L. Wang, Microwave-assisted rapid photocatalytic degradation of malachite green in TiO_2 suspensions: mechanism and pathways, J. Phys. Chem. A 112 (2008) 11172–11177.
[8] S.S. Tahir, N. Rauf, Removal of a cationic dye from aqueous solutions by adsorption onto bentonite clay, Chemosphere 63 (2006) 1842–1848.
[9] M. Zhao, Z. Tang, P. Liu, Removal of methylene blue from aqueous solution with silica nano-sheets derived from vermiculite, J. Hazard. Mater. 158 (2008) 43–51.
[10] V.K. Gupta, A. Mittal, L. Krishnan, V. Gajbe, Adsorption kinetics and column operations for the removal and recovery of malachite green from wastewater using bottom ash, Sep. Purif. Technol. 40 (2004) 87–96.
[11] Z. Bekçi, C. Özveri, Y. Seki, K. Yurdakoç, Sorption of malachite green on chitosan bead, J. Hazard. Mater. 154 (2008) 254–261.
[12] G. Crini, H.N. Peindy, F. Gimbert, C. Robert, Removal of C.I. basic green 4 (malachite green) from aqueous solutions by adsorption using cyclodextrin-based adsorbent: kinetic and equilibrium studies, Sep. Purif. Technol. 53 (2007) 97–110.
[13] L. Ai, H. Huang, Z. Chen, X. Wei, J. Jiang, Activated carbon/$CoFe_2O_4$ composites: facile synthesis, magnetic performance and their potential application for the removal of malachite green from water, Chem. Eng. J. 156 (2010) 243–249.
[14] V.K. Gupta, S.K. Srivastava, D. Mohan, Equilibrium uptake, sorption dynamics, process optimization, and column operations for the removal and recovery of malachite green from wastewater using activated carbon and activated slag, Ind. Eng. Chem. Res. 36 (1997) 2207–2218.
[15] A. Mittal, Adsorption kinetics of removal of a toxic dye, malachite green, from wastewater by using hen feathers, J. Hazard. Mater. B133 (2006) 196–202.
[16] O. Hamdaoui, F. Saoudi, M. Chiha, E. Naffrehoux, Sorption of malachite green by a novel sorbent, dead leaves of plane tree: equilibrium and kinetic modeling, Chem. Eng. J. 143 (2008) 73–84.
[17] W.-T. Tsai, H.-R. Chen, Removal of malachite green from aqueous solution using low-cost chlorella-based biomass, J. Hazard. Mater. 175 (2010) 844–849.
[18] A. Mittal, L. Krishnan, V.K. Gupta, Removal and recovery of malachite green from wastewater using an agricultural waste material, de-oiled soya, Sep. Purif. Technol. 43 (2005) 125–133.
[19] K.V. Kumar, S. Sivanesan, V. Ramamurthi, Adsorption of malachite green onto *Pithophora* sp., a fresh water algae: equilibrium and kinetic modeling, Process Biochem. 40 (2005) 2865–2872.
[20] B. Samiey, A.R. Toosi, Kinetics study of malachite green fading in the presence of TX-100, DTAB and SDS, Bull. Korean Chem. Soc. 30 (2009) 2051–2056.
[21] B. Samiey, A.R. Toosi, Kinetics of malachite green fading in alcohol–water binary mixtures, Int. J. Chem. Kinet. 42 (2010) 508–518.
[22] B. Samiey, A.R. Toosi, Adsorption of malachite green on silica gel: effect of NaCl, pH and 2-propanol, J. Hazard. Mater. 184 (2010) 739–745.
[23] M.G. da Fonseca, C. Airoldi, Phyllosilicate-like structure anchored silylating agents: calorimetric data on divalent cation-aminated centre interactions in the lamellar cavity, J. Chem. Soc., Dalton Trans. (1999) 3687–3692.
[24] J.A.A. Sales, G.C. Petrucelli, F.J.V.E. Oliveira, C. Airoldi, Some features associated with organosilane groups grafted by the sol–gel process onto synthetic talc-like phyllosilicate, J. Colloid Interface Sci. 297 (2006) 95–103.
[25] M.A. Melo Jr., F.J.V.E. Oliveira, C. Airoldi, Novel talc-like nickel phyllosilicates functionalized with ethanolamine and diethanolamine, Appl. Clay Sci. 42 (2008) 130–136.
[26] M.G. da Fonseca, E.C. da Siva Filho, R.S.A. Machado Junior, L.N.H. Arakaki, J.G.P. Espinola, C. Airoldi, J. Solid State Chem. 177 (2004) 2316–2322.
[27] S.L. Burkett, A. Press, S. Mann, Synthesis, characterization, and reactivity of layered inorganic–organic nanocomposites based on 2:1 trioctahedral phyllosilicates, Chem. Mater. 9 (1997) 1071–1073.
[28] S. Mann, S.L. Burkett, S.A. Davis, C.E. Fowler, N.H. Mendelson, S.D. Sims, D. Walsh, N.T. Whilton, Sol–gel synthesis of organized matter, Chem. Mater. 9 (1997) 2300–2310.
[29] S. Mann, Self-assembly and transformation of hybrid nano-objects and nanostructures under equilibrium and non-equilibrium conditions, Nat. Mater. 8 (2009) 781–791.
[30] A.J. Patil, E. Muthusamy, S. Mann, Synthesis and self-assembly of organoclay wrapped biomolecules, Angew. Chem. Int. Ed. 43 (2004) 4928–4933.
[31] A.J. Patil, E. Muthusamy, S. Mann, Fabrication of functional protein–organoclay lamellar nanocomposites by biomolecules-induced assembly of exfoliated aminopropyl-functionalized magnesium phyllosilicates, J. Mater. Chem. 15 (2005) 3838–3843.
[32] K.M. Bromley, A.J. Patil, A.M. Seddon, P. Booth, S. Mann, Bio-functional mesolamellar nanocomposites based on inorganic/polymer interaction in purple membrane (bacteriorhodopsin) films, Adv. Mater. 19 (2007) 2433–2438.
[33] I.L. Lagadic, Schiff base chelate-functionalized organoclays, Micropor. Mesopor. Mater. 95 (2006) 226–233.
[34] Y.-C. Lee, T.-H. Lee, H.-K. Han, W.J. Go, J.-W. Yang, H-J. Shin, Optical properties of fluorescein-labeled organoclay, Photochem. Photobiol. 86 (2010) 520–527.
[35] S.C. Holmström, A.J. Patil, M. Butler, S. Mann, Influence of polymer co-intercalation on guest release from aminopropyl-functionalized magnesium phyllosilicate mesolamellar nanocomposites, J. Mater. Chem. 17 (2007) 3894–3900.
[36] U. Shedbalkar, J.P. Jadhav, Detoxification of malachite green and textile industrial effluent by *Penicillium ochrochloron*, Biotechnol. Bioprocess Eng. 16 (2011) 196–204.
[37] S. Lagergren, About the theory of so-called adsorption of soluble substances, Kungliga Svenska Vetenskapsakademiens Handlingar 24 (1898) 1–39.
[38] Y.S. Ho, G. McKay, Sorption of dye from aqueous solution by peat, Chem. Eng. J. 70 (1998) 115–124.
[39] E. Bulut, M. Ozacar, I.A. Sengil, Adsorption of malachite green onto bentonite: equilibrium and kinetic studies and process design, Micropor. Mesopor. Mater. 115 (2008) 234–246.
[40] M.-X. Zhu, L. Lee, H.-H. Wang, Z. Wang, Removal of an anionic dye by adsorption/precipitation processes using alkaline white mud, J. Hazard. Mater. 149 (2007) 735–741.